

CORE STRUCTURE OF SUPERDISLOCATIONS AND DESTRUCTION OF THE DISLOCATION BARRIERS AFTER HIGH-TEMPERATURE DEFORMATION OF Ti₃Al

Liudmila I. Yakovenkova* and Lidia E. Karkina

Institute of Metal Physics, Ural Branch of RAS, S. Kovalevskaya str. 18

620041 Ekaterinburg, Russia

* E-mail: yakovenkova@imp.uran.ru

Abstract. An electron microscopic analysis of the dislocation structure of the Ti₃Al intermetallic after high-temperature deformation is performed. It is found that the microstructure of the samples deformed at $T = 1073\text{-}1173$ K contains mobile a , $2c+a$ and other c component superdislocations. Experimental data are discussed considering results of the computer simulation of the superdislocation core structure in Ti₃Al.

1. Introduction

Mono- and polycrystalline Ti₃Al alloys are a constituent part of many high-temperature one- and two-phase alloys. Titanium aluminides are light, have a high melting point, and are oxidation resistant. The deformation behavior of Ti₃Al over a wide interval of temperatures has been much investigated experimentally and theoretically. The maximum temperature of their practical applications as a high-temperature material is determined by the temperature and orientation dependences of the deformation characteristics of this alloy. The deformation behavior of Ti₃Al over a wide interval of temperatures has been much investigated experimentally and theoretically (see, for example, [1]).

The smallest yield stress is observed in the case of the prismatic slip. The yield stress $\sigma_y(T)$ monotonically decreases with increasing temperature with a pronounced temperature dependence at lower temperatures, while the elongation is $\varepsilon \sim 250\%$ even at room temperature [1]. In the case of the basal slip, the yield stress at room temperature falls within the interval $\sigma_y \sim 150\div 300$ MPa. At room temperature the elongation equals $\varepsilon \sim 1\text{-}5\%$. It follows from the analysis of the slip geometry that the small value of the elongation in the case of the basal slip is explained by the formation of coarse slip bands of screw a superdislocations which develop shear-type microcracks. The coarse slip and a low plasticity in the basal plane persist up to $T \sim 900$ K. At higher temperatures the slip lines get thinner and the decrease in the yield stress with elevating temperature becomes more obvious in the $\sigma_y(T)$ curve. In the case of the pyramidal slip an anomalous temperature dependence and a peak in the $\sigma_y(T)$ curve are observed in experiments. The maximum value of the yield stress at $T = T_p$ increases by a factor of ~ 1.5 as compared to the corresponding value at room temperature. The elongation is $\varepsilon \sim 2\text{-}7\%$ over this temperature interval. As the temperature grows, the value of $\sigma_y(T)$ decreases considerably above the peak temperature and the plasticity increases. Thus, whatever the type of the active slip system, at $T > 900\text{-}1000$ K the yield stress decreases dramatically with the temperature, while the plasticity is enhanced. Today experimental data

on the character of the dislocation structure in Ti_3Al samples after high-temperature deformation are scarce.

The present study deals with the electron microscopic (TEM) analysis of the dislocation structure in polycrystalline Ti_3Al samples after high-temperature deformation at temperatures $T = 1023\text{-}1273$ K. The temperature evolution of both a superdislocations and c component superdislocations has been studied. Particular emphasis has been placed on the study and theoretical analysis of specific dislocation configurations, which are observed only after deformation at high temperatures. Experimental dates are discussed considering results of the computer simulation of the superdislocation core structure in Ti_3Al .

2. Methodology

Samples of the Ti-25 at.% Al alloy were made by the method described in [2]. Prior to deformation the samples were annealed at $T = 1323$ K for 5 hours and cooled in a furnace. The samples were deformed by pressing to $\sim 3\text{-}7\%$ at temperatures $T = 1073\text{-}1273$ K. The samples were thinned electrolytically to obtain foils for the TEM analysis of the dislocation structure. The $g\mathbf{b}$ -analysis was used for the electron microscopic examination of the dislocation structure. The results of computer simulation were obtained by the molecular dynamics method using the EAM interatomic interaction potentials for Ti_3Al [3].

3. Results and discussion

The analysis of the dislocation structure confirmed the absence of coarse slip bands of screw a superdislocations in basal planes at $T=1073\text{-}1173$ K, which cause the formation of shear-type microcracks. Generally, the TEM analysis showed that a superdislocations were distributed uniformly in a grain. Small dislocation pileups, dislocation junctions and jogs (Fig. 1a) or a tangle-type structure, which are formed during the interaction of dislocations of several slip systems, are observed. Curved, mobile isolated dislocations can be seen too. When determining the Burgers vectors of the dislocations, the dislocation was out of contrast with $\mathbf{g} = 0001$ in these fragments. This is characteristic of a dislocations.

The dislocations D_1 , D_2 and D_3 in Fig. 1a form a dislocation node. The Burgers vectors of the dislocations are $\mathbf{b}_1 = 1/3[\bar{2}110]$ and $\mathbf{b}_2 = 1/3[11\bar{2}0]$. The reaction between the dislocations D_1 and D_2 lead to the formation of the dislocation D_3 with the Burgers vector $\mathbf{b}_3 = 1/3[\bar{1}2\bar{1}0]$:

$$1/3[\bar{2}110] + 1/3[11\bar{2}0] \rightarrow 1/3[\bar{1}2\bar{1}0]. \quad (1)$$

The trace analysis showed that D_2 was a screw dislocation and the dislocation D_1 belonged to the prism plane $(0\bar{1}10)$. The axis of the dislocation D_3 was directed between $[2\bar{1}\bar{1}2] \div [2\bar{1}\bar{1}0]$, i.e. the dislocation D_1 had a nearly screw orientation.

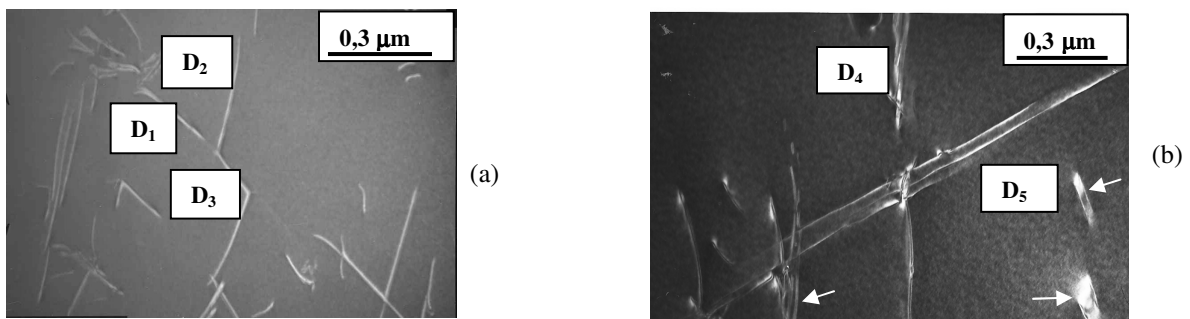


Fig. 1. Bright-field image of a superdislocations in the Ti_3Al alloy (a) after deformation at $T = 1073$ K and dark-field image with $\mathbf{g} = \bar{4}222$ (b) after deformation at $T=1173$ K.

The resulting dislocation D_3 had a 60° orientation and belonged to the basal plane. Thus, the junction in Fig. 1a resulted from the interaction of \mathbf{a} superdislocations belonging to the basal and prism planes. Figure 1b shows a fragment of the Ti_3Al microstructure deformed to $\varepsilon \sim 7\%$ at $T = 1273$ K and this fragment contains 2 types of dislocations marked D_4 and D_5 . The Burgers vector of the dislocations D_4 is $\mathbf{b}_4 = 1/3[\bar{2}110]$. From the trace analysis it was possible to determine the direction of the axis of this dislocation, which coincided with $\mathbf{l}_4 = [\bar{2}110] - [\bar{3}210]$. Thus, \mathbf{a} superdislocation with the Burgers vector \mathbf{b}_4 has an almost screw orientation and belongs to the basal plane (0001). The dislocation D_5 is also \mathbf{a} superdislocation with the Burgers vector $\mathbf{b}_5 = 1/3[1\bar{2}10]$. The trace analysis suggests the direction of the D_5 axis is approximately $\mathbf{l}_5 = [1\bar{2}12] - [3\bar{4}13]$. Thus, \mathbf{a} superdislocation with the Burgers vector \mathbf{b}_5 has a mixed orientation and belongs to the prism plane ($\bar{1}010$). The arrow in Fig. 1b shows a dislocation configuration, which is formed due to the interaction of crossing \mathbf{a} superdislocations having the Burgers vectors \mathbf{b}_4 and \mathbf{b}_5 . The resulting dislocation is split into 2 partial dislocations, which are interconnected by a stacking fault (SF) ribbon in the basal plane. The SF-induced fringe contrast is seen well in Fig. 1b. In addition to this dislocation configuration with SF, other fragments with a wide fringe contrast (shown with arrows in Fig. 1b) can be seen in this figure. The Burgers vectors of the partial dislocations, which limit the stacking fault, cannot be determined, but the observed stacking fault probably is a superstructural intrinsic stacking fault (SISF). Similar dislocation configurations with the SISF in the basal plane were observed in experiments *in situ* [4].

The start and final of a configuration with a SISF formation during the interaction of superdislocations in the basal and prism planes are presented in Fig. 2. The axes of the interacting dislocations were parallel to the interaction of the basal (0001) and prism ($\bar{1}010$) planes; thus, the reaction involved a screw \mathbf{a} superdislocation in the prism plane and a 60° \mathbf{a} superdislocation in the basal plane (Fig. 2a). The computer simulation suggests [3, 5] that \mathbf{a} superdislocations in the prism and basal planes are split into superpartial dislocations limiting the antiphase boundary ribbon by the reactions

$$1/3[\bar{1}2\bar{1}0]_{(\bar{1}010)} = 1/6[\bar{1}2\bar{1}0]_{(\bar{1}010)} + APB_{(\bar{1}010)} + 1/6[\bar{1}2\bar{1}0]_{(\bar{1}010)}, \quad (2)$$

$$1/3[\bar{2}110]_{(0001)} = 1/6[\bar{2}110]_{(0001)} + APB_{(0001)} + 1/6[\bar{2}110]_{(0001)}. \quad (3)$$

Each of the superpartial dislocations, both in the basal plane and the prism plane, is split into two partial dislocations. The partial dislocation in the basal plane limits a complex stacking fault. The shear vector, which equals the Burgers vector of the partial dislocation, corresponds to the local minimum on the γ -surface in the basal plane. The Burgers vectors of the partial dislocations in the prism plane are determined from the computer simulation and correspond to a metastable stacking fault. In the basal plane the reaction of splitting of the superpartial dislocations has the form:

$$1/6[\bar{2}110]_{(0001)} = 1/6[\bar{1}100]_{(0001)} + CSF_{(0001)} + 1/6[\bar{1}010]_{(0001)}, \quad (4)$$

and in the prism plane:

$$1/6[1\bar{2}10]_{(\bar{1}010)} = 1/12[1\bar{2}10]_{(\bar{1}010)} + SF_{(\bar{1}010)} + 1/12[1\bar{2}10]_{(\bar{1}010)}. \quad (5)$$

According to the orientation of the applied external stress (the direction and the sign) relative to the Burgers vectors and slip planes involved in the reaction of dislocations, two configurations are possible and these configurations depend on the sequence of the dislocation reactions between the partial dislocations forming the \mathbf{a} superdislocation in the basal and prism planes. The dislocation reactions which lead to the formation of the configuration with SISF are presented in Fig. 2a. In accordance with (5), the partial dislocations, which belong to the prism plane, can enter into the dislocation reaction with the dislocation $1/6[\bar{1}010]$, which belong to the basal plane. The newly formed stair rod

dislocation is not stable. As a result of successive energetically favorable dislocation reactions, dislocation configurations are formed (Fig. 2b). They are presented in the figure with the SISF limiting the dislocation with the total Burgers vector $1/3[\bar{1}010]$. According to calculations [3], the SISF energy is 78 mJ/m^2 and therefore the formation of a SISF is more energy favorable; the splitting width $D \gg d_1, d_2$ (see Fig. 2b).

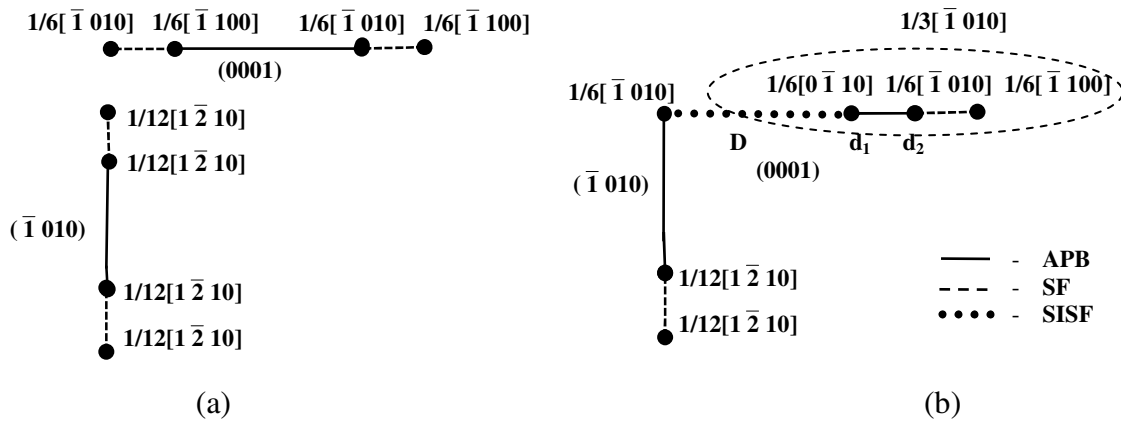


Fig. 2. Start and final of a configuration with a SISF formation during the interaction of superdislocations in basal and prism planes.

The computer simulation of the core structure [3, 5] demonstrated that 30° superpartial dislocations with the Burgers vector $1/6\langle 1\bar{1}00 \rangle$, which are part of the a superdislocations in the basal plane, have a nonplanar core structure. The displacement components of these dislocations are distributed in both the basal plane and the prism plane containing the dislocation axis. For the configuration shown in Fig. 2b, the core structure is nonplanar for the partial dislocations with the Burgers vector $\mathbf{b} = 1/6[\bar{1}100]$ and the axis $\mathbf{l} = [1\bar{2}10]$. These dislocations should move easier at elevated temperatures, explaining the reason why configurations with a superstructural intrinsic stacking fault appear only at high deformation temperatures.

Most of c component dislocations are $2a+c$ superdislocations in Ti_3Al deformed at temperatures $T = 1073\text{-}1273 \text{ K}$. Both c dislocations and $c+a$ superdislocations are observed at $T = 1273 \text{ K}$. The microstructure fragment in Fig. 3 presents interest since it contains atypical dislocations, which cannot be seen at low temperatures. Curved dislocations D_1 are marked in the bright-field image (Fig. 3a). The Burgers vector $\mathbf{b}_1 = 1/3[\bar{1}\bar{1}26]$ of these dislocations was determined. Dislocations D_2 are present in the form of full dislocation loops or coarse dislocation loops of an irregular shape truncated by the foil planes.

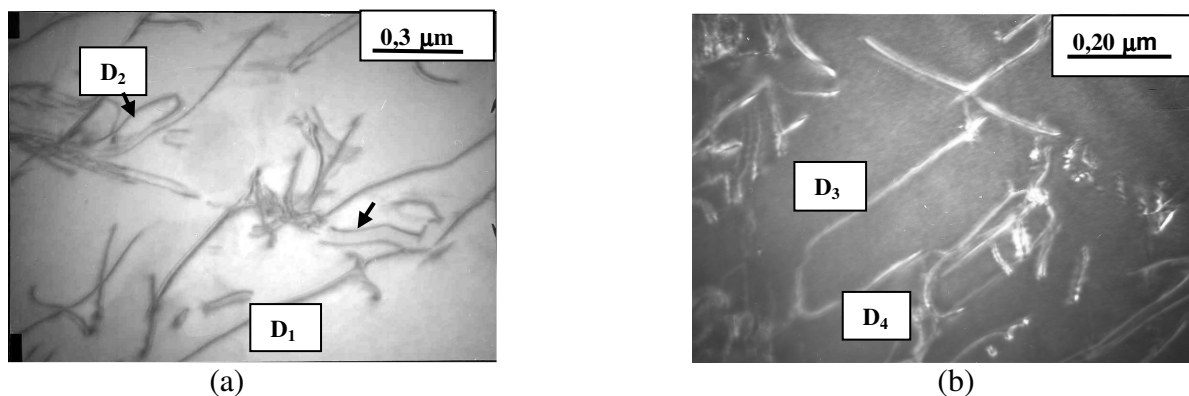


Fig. 3. Fragments of the dislocation structure of Ti_3Al after deformation at $T = 1273 \text{ K}$.

The Burgers vector of dislocations D_2 was determined as $\mathbf{b}_2 = [0001]$; a possible slip plane of these dislocations is the prism plane $(1\bar{2}10)$. The superdislocations with the Burgers vectors $1/3\langle\bar{1}\bar{1}3\rangle$ and $1/3\langle 0\bar{1}13\rangle$ are observed at $T = 1273$ K. The Burgers vectors of dislocation D_3 was determined as $\mathbf{b}_3 = 1/3[\bar{2}113]$; Burgers vectors of dislocation D_4 is $\mathbf{b}_4 = 1/3[0\bar{1}13]$ (Fig. 3b).

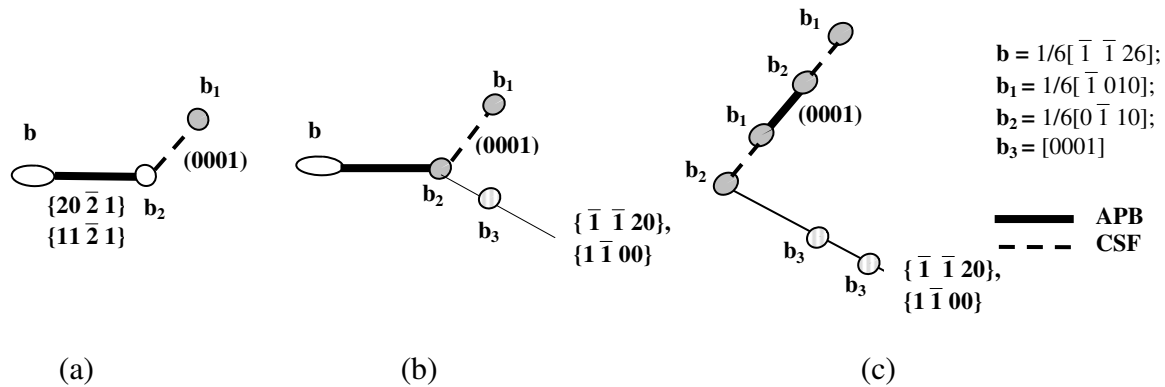
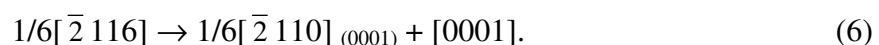


Fig. 4. Scheme of destruction of a dislocation barrier on a $2c+a$ superdislocation in pyramid planes.

The TEM examination showed that over the interval of deformation temperatures studied most of the c component dislocations are $2c+a$ superdislocations, which are mobile in pyramid planes of the I and II types. A peak in the dependence $\sigma_y(T)$ is characteristic of the pyramidal slip. The anomalous increase in the yield stress from room temperature to the peak temperature $T_p \sim 870-1100$ K, when the single crystals are deformed near the orientation $[0001]$, is due to the thermally activated transformation of the $2c+a$ superdislocations from glissile configurations to dislocation barriers. A blocked configuration of a $2c+a$ superdislocation having the edge orientation in the pyramid plane of type II (the axis direction $\langle 1\bar{1}00 \rangle$) or of the nearly edge orientation in the pyramid plane of type I (the axis direction $\langle 11\bar{2}0 \rangle$) is shown schematically in Fig. 4a. The atomistic calculations demonstrated that a blocked configuration, which is characterized by splitting in both the pyramid and basal planes and the formation of a complex stacking fault, has a lower energy than a glissile configuration [6-8]. At temperatures above the peak temperature, these barriers are destructed due to the thermally activated process of recombination of Shockley partial dislocations in the basal plane and subsequent gliding in the pyramid plane. The experimental observation of glissile curved $2c+a$ superdislocations confirms that the barriers are destructible in the pyramid plane over the temperature interval studied (Fig. 3). The destruction activation energy of the barriers is higher than their formation activation energy because of the narrower splitting of the $c+a/2$ superpartial dislocation in the pyramid planes.

The interesting experimental feature of the microstructure at the deformation temperature $T = 1273$ K is the observation of dislocation loops with the Burgers vector $[0001]$ in the prism planes $(1\bar{2}10)$, along with glissile $2c+a$ superdislocations. It is possible to propose an alternative variant of the barrier destruction on $2c+a$ superdislocations in the pyramid planes, as is schematized in Figs. 4b and c in accordance with the dislocation reaction



This model suggests gliding of the $[0001]$ dislocation with the $\langle 1\bar{1}00 \rangle$ axis in the $\{11\bar{2}0\}$ prism plane or with the $\langle 11\bar{2}0 \rangle$ axis in the $\{1\bar{1}00\}$ plane (Fig. 4c). The motion of the $[0001]$ dislocation can be facilitated by stress acting from the second $c+a/2$ superpartial dislocation, which limits the antiphase boundary ribbon in the pyramid plane. The Shockley

partial dislocation in the intersection of the basal and pyramid planes becomes mobile in the basal plane, while the second superpartial dislocation with the Burgers vector $\mathbf{b} = 1/6[\bar{1}\bar{1}26]$ approaches the intersection across the pyramid plane. This dislocation splits emitting the second \mathbf{c} dislocation to the prism plane. The dislocation with the Burgers vector $1/6[\bar{1}\bar{1}20]$ remains in the intersection line. The energy of the dislocation decreases as it splits into Shockley partial dislocations in the basal plane (Fig. 4b). The whole superdislocation with the total Burgers vector $1/3[\bar{1}\bar{1}20]$ becomes mobile in the basal plane. As a result, the pyramid plane of type I or type II is free for the motion of the next $2\mathbf{c}+\mathbf{a}$ superdislocations.

4. Conclusions

1. TEM examination demonstrated that the microstructure of the samples deformed at temperatures $T = 1073\text{-}1273$ K included mobile \mathbf{a} and $2\mathbf{c}+\mathbf{a}$ superdislocations.
2. It was shown that \mathbf{a} superdislocations formed a stepped or tangled structure. Initial stages of the dislocation network formation were observed. Configurations containing a SISF were detected at $T = 1273$ K. It was found that these configurations were formed due to the interaction of \mathbf{a} superdislocations in the basal and prism planes.
3. Separate dislocations with the Burgers vector $[0001]$ in the form of both dislocation loops and those gliding freely in the prism planes were observed at $T = 1273$ K. Superdislocations with the Burgers vectors $1/3\langle 2\bar{1}\bar{1}3 \rangle$ and $1/3\langle 0\bar{1}13 \rangle$ were detected too.
4. The electron microscopic data were compared with results of the computer simulation of the superdislocation core structure in Ti_3Al . A model of the barrier destruction on $2\mathbf{c}+\mathbf{a}$ superdislocations in pyramid planes was proposed.

Acknowledgments

This work was partially supported by RFBR No. 08-02-00022.

References

- [1] L.I. Yakovenkova, L.E. Karkina, *Dislocation core structure and deformation behavior of single-crystal Ti_3Al* . Ekaterinburg; Ural Branch of Russian Academy of Sciences, 2008, 196 p.
- [2] E.V. Panova, L.E. Karkina, E.P. Romanov // *Phys. Met. Metallogr.* **75**, (1993) 453.
- [3] L.I. Yakovenkova, V.V. Kirsanov, L.E. Karkina, A.N. Balashov, M.Ya. Rabovskaya // *Phys. Met. Metallogr.* **89** (2000) 31.
- [4] M. Legros, A. Couret, D. Caillard // *Phil. Mag.* **73A** (1996) 61.
- [5] L.E. Karkina, L.I. Yakovenkova, M.Ya. Rabovskaya // *Phys. Met. Metallogr.* **93** (2002) 32.
- [6] L.I. Yakovenkova, L.E. Karkina, M.Ya. Rabovskaya // *Technical Physics* **73** (2003) 70.
- [7] L.E. Karkina, L.I. Yakovenkova, E.V. Panova, and M.Ya. Rabovskaya // *Phys. Met. Metallogr.* **85** (1998) 150.
- [8] L.I. Yakovenkova, L.E. Karkina, M.Ya. Rabovskaya // *Phys. Met. Metallogr.* **87** (1999) 190.